NATIONAL ADVISORY COMMITTEE FOR AERONAUTICS

TECHNICAL NOTE 3796

THEORETICAL LIFT DUE TO WING INCIDENCE OF SLENDER WING-BODY-TAIL COMBINATIONS AT ZERO ANGLE OF ATTACK

By Alvin H. Sacks

Ames Aeronautical Laboratory
Moffett Field, Calif.

Washington
November 1956

NATIONAL ADVISORY COMMITTEE FOR AERONAUTICS

TECHNICAL NOTE 3796

THEORETICAL LIFT DUE TO WING INCIDENCE OF SLENDER WING-BODY-TAIL COMBINATIONS AT ZERO ANGLE OF ATTACK

By Alvin H. Sacks

SUMMARY

The theoretical lift of a cylindrical afterbody at zero angle of attack due to incidence of the wing is determined by means of slender-body theory. It is assumed that the vortex sheet becomes fully rolled up ahead of the base of the afterbody, and the paths of the vortices in the presence of the body are determined. Since this requires the complete solution of the classical problem of the motion of a two-dimensional vortex pair past a circular cylinder, the analytical solution of that problem is presented herein.

The total lift of a slender wing-body-tail combination due to incidence of the wing is also calculated by making use of the above solution, and lift curves are presented for a variety of tail lengths, span ratios, and body sizes. The lift due to the rolling-up of the vortex sheet is included and is discussed in relation to the calculated results.

It is found that a short afterbody carries positive lift and that a long afterbody carries negative lift. Furthermore, there is a short afterbody length which carries a maximum positive lift and a long afterbody length which carries a maximum negative lift.

INTRODUCTION

The problem of calculating the forces on the body and tail of a slender wing-body-tail combination has received relatively little attention from a theoretical point of view, considering its importance. The reason seems clear when one investigates the possibilities of obtaining analytical solutions for the behavior of the wing wake. There are, however, certain classes of problems in this category which lend themselves to analytical solution. In 1948, for example, Graham (ref. 1) calculated the lift on the tails of some plane wing-tail combinations, and in 1952 Morikawa (ref. 2) investigated the "maximum" wing-body-tail interference by assuming the wing vortices to be fully rolled up and to remain in the plane of the wing and tail. In reference 3 the variations of lift and pitching moment with angle of attack were obtained for a number of slender wing-tail combinations.

The references cited above have one point in common which highlights the principal difficulty underlying all calculations of wing-body-tail interference. Specifically, in no case have the positions of the wing vortices in the presence of the body been calculated analytically. They have on several occasions been obtained numerically (e.g., refs. 4 and 5), but the number of specific configurations treated is relatively small since each case requires a separate numerical calculation.

In the present paper, a class of problems is treated for which an analytical solution will be obtained for the paths of the rolled-up vortices in the presence of the body. In particular, the combinations treated will each consist of a cylindrical body at zero angle of attack with a wing and tail at incidence. This problem is analogous to the classical hydrodynamic problem of the motion of a two-dimensional vortex pair past a circular cylinder. Although the equations of the vortex paths for this latter problem have been given in many places (e.g., refs. 6 and 7), the elapsed time between successive positions has not been expressed analytically to the author's knowledge. The present paper will supply this solution which finally links the three-dimensional slender problem directly to its two-dimensional analogue.

SYMBOLS

a body radius

A aspect ratio

d tail length or afterbody length, $l - x_{TE}$

e distance behind wing trailing edge at which vortex sheet is essentially rolled up

K half the asymptotic spacing of the rolled-up wing vortices, $y_{1_{TE}}\left(\frac{y_{1_{TE}}^2 - a^2}{y_{1_{TE}}^2 + a^2}\right)$

l over-all length of wing-body-tail combination

L lift

r $\sqrt{y^2 + z^2}$

r_o radius of transformed circle corresponding to airplane cross section

s local semispan of wing or tail

s_o maximum semispan of wing (at $x = x_{TE}$)

s_1 maximum semispan of tail (at $x = l$)

S_w exposed areas of both wing panels

U_o flight speed in the negative x direction

v_1, w_1 components of velocity of the starboard rolled-up vortex in the positive y and z directions

x_{TE+} distance from airplane nose to position immediately behind wing trailing edge

xyz Cartesian coordinates fixed in the body as illustrated in sketch (a)

y_1, z_1 y and z coordinates of starboard rolled-up vortex

α angle of attack of the body (taken as zero throughout)

Γ strength of one rolled-up vortex shed from the wing

Γ_k circulation of kth external (free) vortex, positive counterclockwise (looking upstream)

Γ_w circulation on the wing

δ incidence angle of surface relative to the body axis (and flight direction), radians

ζ $y + iz$

ζ_k position of kth external (free) vortex, $y_k + iz_k$

ρ fluid mass density

σ complex coordinate in transformed circle plane

σ_k position of kth external vortex in σ plane

σ_{k_r} position of kth external vortex relative to its image in the transformed circle, $\sigma_k - \frac{r_o^2}{\bar{\sigma}_k}$

$\Delta\varphi$ difference in potential between upper and lower surfaces

Subscripts

A afterbody (with no tail)

I due to vortex interference

W wing (forward surface)

BT body-tail combination (isolated segment of airplane behind wing trailing edge)

WB wing-body combination (segment of airplane ahead of wing trailing edge)

T tail (rear surface)

TE wing trailing edge

Special Notations

$\mathbf{R}$ real part

$\bar{(\ )}$ complex conjugate of ( )

ANALYSIS

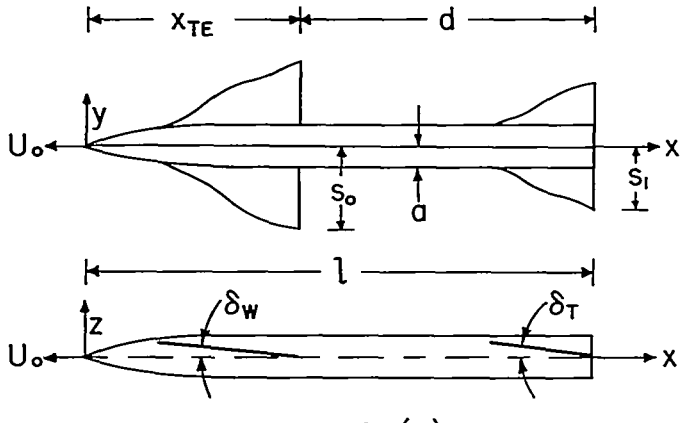

Sketch (a)

The class of slender wing-body-tail combinations to be treated in the present analysis is illustrated in sketch (a). The body is a circular cylinder of radius a behind the wing trailing edge. The wing and tail are at incidence to the body as shown, but the body is aligned with the flight direction. The wing and tail are thin flat plates whose straight trailing edges lie in the planes $x = x_{TE}$ and $x = l$ as shown above.

Formulas for the Lift

In reference 8, it was shown that the interference lift of a slender wing-body-tail combination in steady straight flight is given by

$$L_I = \rho U_o \mathbf{R}\left(\sum_{k=1}^{m} \Gamma_k \sigma_{k_r}\right)_{x=l} - \rho U_o \mathbf{R}\left(\sum_{k=1}^{m} \Gamma_k \sigma_{k_r}\right)_{x=x_{TE+}} \tag{1}$$

where σ_{k_r} represents the (complex) distance between the kth shed vortex and its image in the transformed circle plane, m is the number of shed vortices, and $\mathbf{R}$ signifies the real part. Since the body of the combination to be treated here is of circular cross section, the transformation from the physical (ζ) plane to the circle (σ) plane immediately behind the wing trailing edge is simply $\zeta = \sigma$. In this case it is easy to verify that the last term of equation (1) is actually equal to the lift of the wing-body combination ahead of the wing trailing edge. Thus, if the vortex sheets leave the wing panels as flat sheets, we have at $x = x_{TE+}$

$$\sigma_k = \zeta_k = y$$

and

$$\Gamma_k = -\frac{d\Gamma}{dy}\,dy$$

Hence

$$\rho U_o \mathbf{R}\left(\sum_{k=1}^{\infty} \Gamma_k \sigma_{k_r}\right)_{x=x_{TE+}} = -\rho U_o \int_{-s_o}^{+s_o} \frac{d\Gamma}{dy}\, y\, dy \tag{2}$$

or, after an integration by parts,

$$\rho U_o \mathbf{R}\left(\sum_{k=1}^{\infty} \Gamma_k \sigma_{k_r}\right)_{x=x_{TE+}} = \rho U_o \int_{-s_o}^{+s_o} \Gamma\, dy = \rho U_o \int_{-s_o}^{+s_o} \Delta\varphi_{TE} dy \tag{3}$$

which is just the slender-body formula for the lift of the wing-body combination ahead of the wing trailing edge (see ref. 9).

By virtue of equation (3), then, the interference lift of equation (1) can be expressed as

$$L_I = \rho U_o \mathbf{R}\left(\sum_{k=1}^{m} \Gamma_k \sigma_{k_r}\right)_{x=l} - L_{WB} \tag{4}$$

and the total lift of the wing-body-tail combination is given by

$$L = L_{WB} + L_{BT} + L_I = \rho U_o \mathbf{R}\left(\sum_{k=1}^{m} \Gamma_k \sigma_{k_r}\right)_{x=l} + L_{BT} \tag{5}$$

Now, since both L_{WB} and L_{BT} are already known from slender-body theory (see ref. 10), the problem of the present analysis is really that of determining the complex quantity $\sum_{k=1}^{m} \Gamma_k \sigma_{k_r}$ at the base of the configuration. For the plane wing-body-tail combinations to be considered in this treatment (see sketch (a)), the mapping function of the base cross section can be expressed as

$$\sigma = \frac{1}{2}\left[\zeta + \frac{a^2}{\zeta} + \sqrt{\left(\zeta + \frac{a^2}{\zeta}\right)^2 - 4r_o^2}\right] \tag{6}$$

The radius r_o of the transformed circle is given by

$$r_o = \frac{1}{2}\left(s_1 + \frac{a^2}{s_1}\right) \tag{7}$$

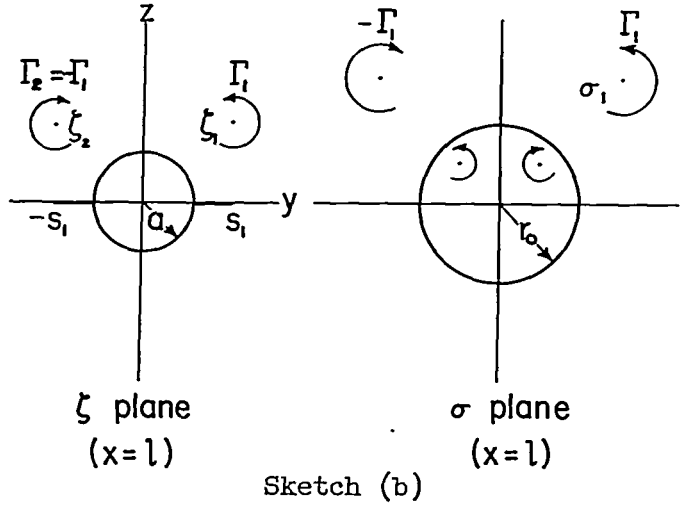

Sketch (b)

where s_1 is the semispan of the trailing edge (sketch (b)).

Now since the complex distance σ_{1_r} between the starboard rolled-up vortex and its image is given by

$$\sigma_{1_r} = \sigma_1 - \frac{r_o^2}{\bar{\sigma}_1} \tag{8}$$

we find from equations (6) and (7) that

$$\sigma_{1_r} = \frac{1}{2}\left[\zeta_1 + \frac{a^2}{\zeta_1} - \bar{\zeta}_1 - \frac{a^2}{\bar{\zeta}_1} + \sqrt{\left(\bar{\zeta}_1 + \frac{a^2}{\bar{\zeta}_1}\right)^2 - \left(s_1 + \frac{a^2}{s_1}\right)^2} + \sqrt{\left(\zeta_1 + \frac{a^2}{\zeta_1}\right)^2 - \left(s_1 + \frac{a^2}{s_1}\right)^2}\right] \tag{9}$$

Furthermore, by symmetry, (sketch (b))

$$\Gamma_2 = -\Gamma_1 = -\Gamma$$

and

$$\zeta_2 = -\bar{\zeta}_1$$

Therefore, the quantity $\sum_{k=1}^{2} \Gamma_k \sigma_{k_r}$ at the base of the configuration can be expressed as

$$\left(\sum_{k=1}^{2} \Gamma_k \sigma_{k_r}\right)_{x=l} = \Gamma\left(\sigma_{1_r} - \sigma_{2_r}\right)_{x=l} = 2\Gamma \mathbf{R} \sqrt{\left(\zeta_{1_l} + \frac{a^2}{\zeta_{1_l}}\right)^2 - \left(s_1 + \frac{a^2}{s_1}\right)^2} \tag{10}$$

With this expression, equations (4) and (5) become[1]

$$L_I = 2\rho U_o \Gamma \mathbf{R} \sqrt{\left(\zeta_{1_l} + \frac{a^2}{\zeta_{1_l}}\right)^2 - \left(s_1 + \frac{a^2}{s_1}\right)^2} - L_{WB} \tag{11}$$

and

$$L = 2\rho U_o \Gamma \mathbf{R} \sqrt{\left(\zeta_{1_l} + \frac{a^2}{\zeta_{1_l}}\right)^2 - \left(s_1 + \frac{a^2}{s_1}\right)^2} + L_{BT} \tag{12}$$

The only two quantities in the above expressions that are not immediately known are the strength Γ of the starboard rolled-up vortex and its position at the tail trailing edge ζ_{1_l}. The remainder of the analysis will therefore be devoted to the determination of these two quantities.

[1]The procedure for taking the real part of the square root without ambiguity has been given in Appendix B of reference 8.

Strengths and Initial Positions of the Rolled-Up Vortices

The spanwise circulation distribution over the wing of the combination of sketch (a) was given in a transformed plane in equation (59) of reference 10 and can be expressed in the physical yz plane as

$$\Gamma_W \equiv \Delta\varphi_W = \frac{2U_o\delta_W}{\pi}\left\{\left(y+\frac{a^2}{y}\right)\tanh^{-1}\left[\frac{2a}{y+\frac{a^2}{y}}\sqrt{\frac{\left(s+\frac{a^2}{s}\right)^2-\left(y+\frac{a^2}{y}\right)^2}{\left(s+\frac{a^2}{s}\right)^2-4a^2}}\right]-\right.$$

$$2a\tanh^{-1}\sqrt{\frac{\left(s+\frac{a^2}{s}\right)^2-\left(y+\frac{a^2}{y}\right)^2}{\left(s+\frac{a^2}{s}\right)^2-4a^2}}+\frac{\pi}{2}\sqrt{\left(s+\frac{a^2}{s}\right)^2-\left(y+\frac{a^2}{y}\right)^2}+$$

$$\left.\sqrt{\left(s+\frac{a^2}{s}\right)^2-\left(y+\frac{a^2}{y}\right)^2}\cos^{-1}\left(\frac{2a}{s+\frac{a^2}{s}}\right)\right\} \qquad (13)$$

It will be assumed in the present analysis that the positions of the rolled-up vortices can be determined with good accuracy by considering the vortex sheets as fully rolled up immediately behind the wing trailing edge. In reference 11 this assumption was shown to be justified for the case of no body ($a = 0$). Therefore we shall determine the strength and position of a rolled-up vortex at the wing trailing edge to replace the flat sheet having the above distribution of circulation.

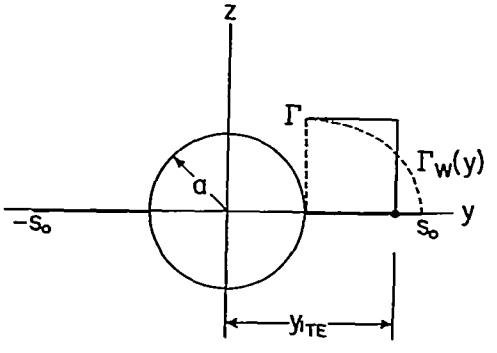

Sketch (c)

The position $y_{1_{TE}}$ and strength Γ of the rolled-up starboard vortex at the wing trailing edge are found by requiring that the lift impulse supplied by the wing panel be the same for the rolled-up vortices as for the flat sheets. Thus, in view of sketch (c), the known expression of slender-body theory for the lift of both panels yields

$$\frac{L_W}{\frac{1}{2}\rho U_o^2} = \frac{4}{U_o}\int_a^{s_o} \Delta\varphi_{W_{TE}}\,dy = \frac{4}{U_o}\int_a^{s_o} \Gamma_{W_{TE}}\,dy = \frac{4}{U_o}\,\Gamma\left(y_{1_{TE}} - a\right) \tag{14}$$

so that

$$y_{1_{TE}} = \frac{L_W}{2\rho U_o \Gamma} + a \tag{15}$$

The value of Γ is seen from sketch (c) to be equal to Γ_W at $y = a$ and $s = s_o$ and is therefore obtained directly from equation (13). The resulting expression for Γ is

$$\Gamma = \frac{2U_o\delta_W s_o}{\pi}\left(1 - \frac{a^2}{s_o^2}\right)\left[\frac{\pi}{2} + \cos^{-1}\left(\frac{2\,\frac{a}{s_o}}{1+\frac{a^2}{s_o^2}}\right)\right] \tag{16}$$

The lift of both wing panels of the combination has been given in reference 10 and for the present case reduces to

$$L_W = \frac{1}{2}\rho U_o^2 \delta_W \left\{ \frac{\pi}{2}\left(\frac{s_o^2 - a^2}{s_o}\right)^2 - 4\,\frac{a}{s_o}\left(s_o^2 - a^2\right) + 2\left(\frac{s_o^4 + a^4}{s_o^2}\right)\cos^{-1}\left(\frac{2as_o}{s_o^2 + a^2}\right) + \right.$$

$$8a^2\cot^{-1}\frac{a}{s_o} + \frac{2}{\pi}\left(\frac{s_o^4 + a^4}{s_o^2}\right)\left[\cos^{-1}\left(\frac{2as_o}{s_o^2 + a^2}\right)\right]^2 -$$

$$\frac{8}{\pi}\,\frac{a}{s_o}\left(s_o^2 - a^2\right)\cos^{-1}\left(\frac{2as_o}{s_o^2 + a^2}\right) + \frac{16}{\pi}\,a^2\cos^{-1}\left(\frac{2as_o}{s_o^2 + a^2}\right)\cot^{-1}\frac{a}{s_o} -$$

$$\left.\frac{16}{\pi}\,a^2\left(\cot^{-1}\frac{a}{s_o}\right)^2 - \frac{8}{\pi}\,a^2 \ln\frac{4a^2 s_o^2}{\left(s_o^2 + a^2\right)^2} - \pi a^2 \right\} \tag{17}$$

With equation (16) and the above expression, then, the position of the starboard vortex at the trailing edge is obtained directly from equation (15). The resulting lateral position in wing semispans is

$$\frac{y_{1_{TE}}}{s_o} = \frac{\left(1-\frac{a^2}{s_o^2}\right)\left[\frac{\pi}{2}\left(1-\frac{a^2}{s_o^2}\right)-4\frac{a}{s_o}\right]+\left[2\left(1+\frac{a^4}{s_o^4}\right)-\frac{8}{\pi}\frac{a}{s_o}\left(1-\frac{a^2}{s_o^2}\right)+4\frac{a^2}{s_o^2}\right]\cos^{-1}\left(\frac{2\frac{a}{s_o}}{1+\frac{a^2}{s_o^2}}\right)+\left[\frac{2}{\pi}\left(1+\frac{a^4}{s_o^4}\right)+\frac{4}{\pi}\frac{a^2}{s_o^2}\right]\left[\cos^{-1}\left(\frac{2\frac{a}{s_o}}{1+\frac{a^2}{s_o^2}}\right)\right]^2}{\frac{8}{\pi}\left(1-\frac{a^2}{s_o^2}\right)\left[\frac{\pi}{2}+\cos^{-1}\left(\frac{2\frac{a}{s_o}}{1+\frac{a^2}{s_o^2}}\right)\right]} - \frac{2\frac{a^2}{s_o^2}\ln\left(\frac{2\frac{a}{s_o}}{1+\frac{a^2}{s_o^2}}\right)}{\left(1-\frac{a^2}{s_o^2}\right)\left[\frac{\pi}{2}+\cos^{-1}\left(\frac{2\frac{a}{s_o}}{1+\frac{a^2}{s_o^2}}\right)\right]}+\frac{a}{s_o} \qquad (18)$$

This equation is plotted in figure 1. Thus the strength and position of the rolled-up vortex at the wing trailing edge are given by equations (16) and (18), and the remainder of the analysis will be concerned with determining the vortex positions at some distance behind the wing. It will then be possible to calculate the interference lift and the total lift of the wing-body-tail combination of sketch (a) directly by means of equations (11) and (12).

Determination of the Vortex Positions Downstream

If we denote by d the distance behind the wing trailing edge and by t_1 the time for the airplane to travel that distance at the constant speed U_o, then we may write

$$d = U_o\int_0^{t_1} dt = U_o\int_{y_{1_{TE}}}^{y_1}\frac{dy}{dy/dt} = U_o\int_{y_{1_{TE}}}^{y_1}\frac{dy}{v_1} \qquad (19)$$

where y_1 is the lateral position of the starboard vortex at distance d behind the wing and v_1 is its component of velocity in the y direction induced by the port vortex and by the image vortices within the body. Thus equation (19), if it can be integrated, offers a direct relationship between the lateral position y_1 of the starboard vortex and the corresponding distance d behind the wing trailing edge.

The induced velocity component v_1 can perhaps most easily be expressed as the real part of the derivative of the appropriate complex potential, which is the total potential minus the potential due to the vortex in question. Thus (see sketch (d))

$$v_1 = \mathbf{R}(v_1 - iw_1) = \mathbf{R}\left\{\frac{d}{d\zeta}\left[\frac{i\Gamma}{2\pi}\ln\frac{\left(\zeta - \frac{a^2}{\bar{\zeta}_1}\right)\left(\zeta + \bar{\zeta}_1\right)}{\left(\zeta + \frac{a^2}{\bar{\zeta}_1}\right)}\right]\right\}_{\zeta=\zeta_1} \tag{20}$$

where $\zeta = y + iz$. Upon carrying out the operations indicated, one finds after some algebraic manipulation that v_1 can be expressed in the form

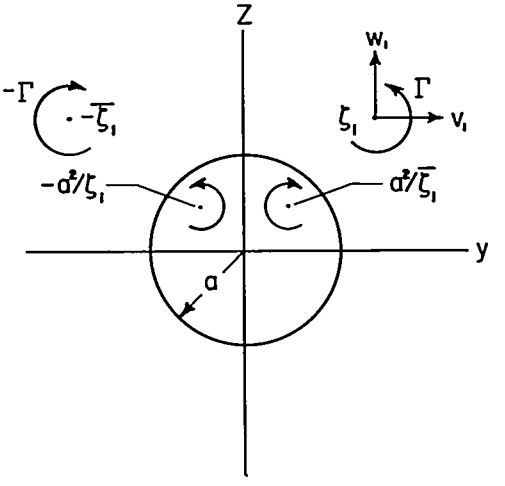

Sketch (d)

$$v_1 = \frac{2\Gamma a^2}{\pi(r^2 - a^2)}\left[\frac{y^2 z}{(r^2 - a^2)^2 + 4a^2y^2}\right] \tag{21}$$

where $r^2 = y^2 + z^2$.

Now the integration of equation (19) is to be performed along the path of the vortex in the yz plane. That is, we must have a relation between y and z which defines the projection of the vortex path on the yz plane. Expressions for the required path have been given in many places (e.g., ref. 6, pp. 330-331) and can be written in the coordinate system of sketch (d) as

$$r^2 - a^2 = \frac{2Kay}{\sqrt{y^2 - K^2}} \tag{22}$$

where K is a constant which depends on the initial position $y_{1_{TE}}$ and on the body radius a. We shall now write z in the form

$$z = -\sqrt{r^2 - y^2} = -\sqrt{(r^2 - a^2) + a^2 - y^2} \tag{23}$$

noting that the minus sign is required since z is to have only negative values for the present problem. That is, the vortex starts at the trailing edge ($z = 0$) as shown in sketch (c) and moves downward as can be seen from the directions of rotation shown in sketch (d). Now, making use of equation (22) to note that

$$(r^2 - a^2)^2 + 4a^2y^2 = \frac{4a^2y^4}{y^2 - K^2} \tag{24}$$

we find that, after simplification, equation (21) for the velocity component v_1 can be expressed as

$$v_1 = -\frac{\Gamma(y^2 - K^2)^{5/4}\sqrt{2Kay + (a^2 - y^2)\sqrt{y^2 - K^2}}}{4\pi a y^3 K} \tag{25}$$

Thus the distance d of equation (19) can finally be written as

$$d = -\frac{4\pi U_o a K}{\Gamma}\int_{y_{1_{TE}}}^{y_1} \frac{y^3 dy}{(y^2 - K^2)^{5/4}\sqrt{2Kay + (a^2 - y^2)\sqrt{y^2 - K^2}}} \tag{26}$$

This then is the integral to be evaluated.

It can easily be verified that the transformation

$$y = \left(\frac{\tau + 1}{2\sqrt{\tau}}\right)K \tag{27}$$

reduces equation (26) to the form

$$d = -\frac{2\pi U_o a K^2}{\Gamma}\int_{\tau_o}^{\tau_l} \frac{(\tau + 1)^3 d\tau}{\tau(\tau - 1)\sqrt{\alpha_o\tau^4 + \alpha_1\tau^3 + \alpha_2\tau^2 + \alpha_3\tau + \alpha_4}} \tag{28}$$

where

$\alpha_o = \alpha_4 = -K^2$

$\alpha_1 = 8Ka + 4a^2$

$\alpha_2 = 2K^2 - 8a^2$

$\alpha_3 = 4a^2 - 8Ka$

The above integral is an incomplete elliptic integral of the third kind and can be evaluated by means of reference 12 in terms of the roots of the fourth degree polynomial inside the radical. Thus, if we divide out the rational fraction in the integral, equation (28) becomes

$$d = -\frac{2\pi U_o a K^2}{\Gamma}\left[\int_{\tau_o}^{\tau_l}\frac{\tau\,d\tau}{\sqrt{P(\tau)}} + 4\int_{\tau_o}^{\tau_l}\frac{d\tau}{\sqrt{P(\tau)}} - \int_{\tau_o}^{\tau_l}\frac{d\tau}{\tau\sqrt{P(\tau)}} + 8\int_{\tau_o}^{\tau_l}\frac{d\tau}{(\tau-1)\sqrt{P(\tau)}}\right] \tag{29}$$

where

$$P(\tau) = \alpha_o\tau^4 + \alpha_1\tau^3 + \alpha_2\tau^2 + \alpha_3\tau + \alpha_4$$

It can be shown that $\tau = 1$ is a root of $P(\tau)$ so that all four of the integrals in equation (29) are basic types which are integrated in reference 12, pages 95 to 137.

Since $\tau = 1$ is a root of the polynomial $P(\tau)$, the remaining roots can be found by solving the cubic equation

$$\frac{P(\tau)}{-K^2(\tau-1)} \equiv \tau^3 - \left(\frac{4a^2 + 8Ka - K^2}{K^2}\right)\tau^2 + \left(\frac{4a^2 - 8Ka - K^2}{K^2}\right)\tau - 1 = 0 \tag{30}$$

The solution is well known and can be found in many books (see, e.g., ref. 13, pp. 9 and 10) for all cases, but it can be shown, following the notation of reference 13 that here

$$\left.\begin{aligned} 3p &= \frac{1}{3}\left(\frac{K^2 - 8Ka - 4a^2}{K^2}\right)^2 - \left(\frac{4a^2 - 8Ka - K^2}{K^2}\right) > 0 \\ \text{and} \\ 2q &= \frac{1}{3}\left(\frac{K^2 - 8Ka - 4a^2}{K^2}\right)\left(\frac{4a^2 - 8Ka - K^2}{K^2}\right) - \frac{2}{27}\left(\frac{K^2 - 8Ka - 4a^2}{K^2}\right)^3 + 1 > 0 \end{aligned}\right\} \tag{31}$$

so that only two cases need to be considered. If $q^2 > p^3$, there is one real root and two conjugate complex roots given by

$$\left.\begin{aligned}
\tau_1 &= 2\sqrt{p}\cosh\left[\frac{1}{3}\cosh^{-1}\left(\frac{q}{p^{3/2}}\right)\right] - \frac{1}{3}\left(1 - 8\frac{a}{K} - 4\frac{a^2}{K^2}\right) \\
\tau_2 &= -\sqrt{p}\cosh\left[\frac{1}{3}\cosh^{-1}\left(\frac{q}{p^{3/2}}\right)\right] + i\sqrt{3p}\sinh\left[\frac{1}{3}\cosh^{-1}\left(\frac{q}{p^{3/2}}\right)\right] - \frac{1}{3}\left(1 - 8\frac{a}{K} - 4\frac{a^2}{K^2}\right) \\
\tau_3 &= -\sqrt{p}\cosh\left[\frac{1}{3}\cosh^{-1}\left(\frac{q}{p^{3/2}}\right)\right] - i\sqrt{3p}\sinh\left[\frac{1}{3}\cosh^{-1}\left(\frac{q}{p^{3/2}}\right)\right] - \frac{1}{3}\left(1 - 8\frac{a}{K} - 4\frac{a^2}{K^2}\right)
\end{aligned}\right\} \quad (32)$$

On the other hand, if $q^2 < p^3$, there are three real roots given by

$$\left.\begin{aligned}
\tau_1' &= 2\sqrt{p}\cos\left[\frac{1}{3}\cos^{-1}\left(\frac{q}{p^{3/2}}\right)\right] - \frac{1}{3}\left(1 - 8\frac{a}{K} - 4\frac{a^2}{K^2}\right) \\
\tau_2' &= -\sqrt{p}\cos\left[\frac{1}{3}\cos^{-1}\left(\frac{q}{p^{3/2}}\right)\right] + \sqrt{3p}\sin\left[\frac{1}{3}\cos^{-1}\left(\frac{q}{p^{3/2}}\right)\right] - \frac{1}{3}\left(1 - 8\frac{a}{K} - 4\frac{a^2}{K^2}\right) \\
\tau_3' &= -\sqrt{p}\cos\left[\frac{1}{3}\cos^{-1}\left(\frac{q}{p^{3/2}}\right)\right] - \sqrt{3p}\sin\left[\frac{1}{3}\cos^{-1}\left(\frac{q}{p^{3/2}}\right)\right] - \frac{1}{3}\left(1 - 8\frac{a}{K} - 4\frac{a^2}{K^2}\right)
\end{aligned}\right\} \quad (33)$$

In order to use the tables of elliptic integrals in reference 12, we must order the real roots of the polynomial $P(\tau)$ with respect to one another and with respect to the limits of integration. Now from equation (27), solving for τ, we find that the limits of integration are

$$\left.\begin{aligned}\tau_0 &= -1 + 2\frac{y_{1_{TE}}^2}{K^2} + 2\frac{y_{1_{TE}}}{K}\sqrt{\frac{y_{1_{TE}}^2}{K^2} - 1} \\ \tau_1 &= -1 + 2\frac{y_1^2}{K^2} + 2\frac{y_1}{K}\cdot\sqrt{\frac{y_1^2}{K^2} - 1}\end{aligned}\right\} \tag{34}$$

where $y_{1_{TE}}$ is the lateral position of the centroid of vorticity at the wing trailing edge and is given by equation (18). The position y_1 is of course a variable depending on the distance d downstream. It should be noted that the plus sign was chosen on the above square roots since the minus sign leads in some cases to negative values of $P(\tau)$ which give imaginary values for the distance d and therefore have no meaning.

Now, once the value of K is determined, the roots of the polynomial $P(\tau)$ are given by equations (31) to (33), and the limits of integration are given by equation (34). Therefore, the final step required before the integrations of equation (29) can be carried out is the determination of K. This has been done in reference 6, page 330, in terms of the distance between the vortices and their images, and, since K is a constant, we need only know the vortex positions at any one station, say the trailing edge of the wing, in order to evaluate it. Thus, denoting the positions of the starboard vortex and its image at $d = 0$ as $y_{1_{TE}}$ and $y_{1_{TE}} - \frac{a^2}{y_{1_{TE}}}$, respectively, we find directly from the above reference that[2]

$$K = y_{1_{TE}}\left(\frac{y_{1_{TE}}^2 - a^2}{y_{1_{TE}}^2 + a^2}\right) \tag{35}$$

We are now in a position to calculate all the roots and the limits of integration and therefore to order all the real roots as required.

The roots of $P(\tau)$ are plotted in figure 2 and it is found that if all the roots are real (eq. (33)) then they are ordered as follows:

$$\tau_1' > \tau_1 > 1 > \tau_2' > \tau_3' \tag{36}$$

---

[2]It is interesting to note that (see ref. 6) the constant K is half the asymptotic spacing of the free vortices; that is, the spacing for large d.

It can be seen from figure 2(b) that two of the roots become equal at about $K/a = 0.296$. For larger values of K/a, two roots are complex. In this case (eq. (32)) we need only know that

$$\tau_1 > \tau_l > 1 \tag{37}$$

Furthermore, it is found that the lower limit of integration τ_o is actually equal to τ_1' if all the roots are real and is equal to τ_1 if two roots are complex, so that the lower limit is a root of $P(\tau)$ in all cases.

With the above information, equation (29) for the distance d behind the wing trailing edge can be expressed in two alternative forms depending on whether the roots of $P(\tau)$ are all real or not. Thus, if $q^2 > p^3$, where p and q are defined by equation (31), then $P(\tau)$ can be written in the form

$$\begin{aligned} P(\tau) &= -K^2(\tau - 1)(\tau - \tau_1)(\tau - \tau_2)(\tau - \tau_3) \\ &= K^2(\tau - 1)(\tau_1 - \tau)(\tau - \tau_2)(\tau - \tau_3) \end{aligned} \tag{38}$$

where τ_1, τ_2, and τ_3 are given by equation (32) and are ordered according to equation (37). Hence we can write equation (29) for this case in the form

$$d = -\frac{2\pi U_o a K}{\Gamma}\left[\int_{\tau_1}^{\tau_l} \frac{\tau\, d\tau}{\sqrt{(\tau-1)(\tau_1-\tau)(\tau-\tau_2)(\tau-\tau_3)}} + 4\int_{\tau_1}^{\tau_l} \frac{d\tau}{\sqrt{(\tau-1)(\tau_1-\tau)(\tau-\tau_2)(\tau-\tau_3)}} - \int_{\tau_1}^{\tau_l} \frac{d\tau}{\tau\sqrt{(\tau-1)(\tau_1-\tau)(\tau-\tau_2)(\tau-\tau_3)}} + 8\int_{\tau_1}^{\tau_l} \frac{d\tau}{(\tau-1)\sqrt{(\tau-1)(\tau_1-\tau)(\tau-\tau_2)(\tau-\tau_3)}}\right] \tag{39}$$

On the other hand if $q^2 < p^3$, then the expressions corresponding to equations (38) and (39) are found by simply substituting the primed roots given in equation (33) for the unprimed roots in the above expressions.

The integrals of equation (39) can all be found in the tables of reference 12, but extreme caution must be used in picking the proper forms considering the ordering in equations (36) and (37) for the two cases. For some of the integrals, the limits of integration will have to be

interchanged with a corresponding change in sign, and for others it will be necessary to divide the integral into two parts, as for instance,

$$\int_{\tau_1}^{\tau_l} = \int_{\tau_1}^{1} + \int_{1}^{\tau_l} = \int_{1}^{\tau_l} - \int_{1}^{\tau_1}$$

for the case of two complex roots. In order to avoid any possible confusion in selecting the proper forms, we shall enumerate here the formulas of reference 12 to be used. For the case of all real roots, the four integrals of equation (39) are given respectively by formulas 257.11, 257.00, 257.12, and 257.29. For two roots complex, the corresponding integrals are given by formulas 259.03, 259.00, 259.04, and 259.07. With these formulas, then, equation (39) gives a direct relationship between the lateral position y_1 of the starboard vortex and the corresponding downstream distance d. Equation (39) is also of interest in connection with the classical problem in hydrodynamics of the motion of a two-dimensional vortex pair past a circular cylinder. In view of equation (19), equation (39) gives the time elapsed between any two successive positions of the vortices.

Now if we divide equation (35) by equation (16) we obtain the quantity $\frac{K}{\Gamma}$ as a function of $\frac{a}{s_o}$ and of $\frac{y_{1_{TE}}}{s_o}$ which is also a function of $\frac{a}{s_o}$ as given by equation (18). Therefore, since τ_l is a function of $\frac{y_1}{K}$ (eq. (34)), we can write equation (39) in a more convenient form as

$$\delta_W \frac{d}{s_o} = f\left(\frac{y_1}{K}, \frac{a}{s_o}\right) \tag{40}$$

which gives us curves of $\delta_W \frac{d}{s_o}$ vs. $\frac{y_1}{K}$ for various chosen ratios of body radius to wing semispan. Such curves are presented in figure 3 and curves of $\frac{a}{K}$ and $\left(\frac{a}{s_o}\right)\left(\frac{KU_o\delta_W}{\Gamma}\right)$ against $\frac{a}{s_o}$ are given in figures 4 and 5.

RESULTS AND DISCUSSION

In the remainder of this report we shall apply the foregoing analysis to the calculation of lift for several different configurations. The first calculations will be concerned solely with wing-body-afterbody

combinations having no tail. Thus we set $s_1 = a$ in equations (11) and (12) to obtain respectively for the lift of the afterbody and the lift of the combination

$$L_A = 2\rho U_o \Gamma \mathbf{R}\left(\zeta_{1_l} - \frac{a^2}{\zeta_{1_l}}\right) - L_{WB} \tag{41}$$

and

$$L = 2\rho U_o \Gamma \mathbf{R}\left(\zeta_{1_l} - \frac{a^2}{\zeta_{1_l}}\right) \tag{42}$$

The wing-body lift L_{WB} with no afterbody is given in reference 10 as

$$L_{WB} = \frac{\pi}{2}\rho U_o^2 \delta_W s_o^2 \left(1 - \frac{a^2}{s_o^2}\right)^2 \left[1 - \frac{4\frac{a}{s_o}}{\pi\left(1 - \frac{a^2}{s_o^2}\right)} + \frac{2}{\pi}\left(\frac{1 + \frac{a^2}{s_o^2}}{1 - \frac{a^2}{s_o^2}}\right)^2 \cos^{-1}\left(\frac{2\frac{a}{s_o}}{1 + \frac{a^2}{s_o^2}}\right)\right] \tag{43}$$

Now, with equation (43), with the results of the foregoing section as summarized in figure 3, with equation (16) for Γ, and with equations (22) and (23) for z, it is a simple matter to calculate the afterbody lift and total lift from equations (41) and (42) for various afterbody lengths and body-diameter to wing-span ratios. The results are presented in figures 6 to 9 and it can be seen that there is a value of $\delta_W \frac{d}{s_o}$ for which the (negative) lift on the afterbody is a maximum for a given ratio of body radius to wing semispan (fig. 6). Similarly, for a given $\delta_W \frac{d}{s_o}$, there is a value of $\frac{a}{s_o}$ for which the afterbody lift is a negative maximum, as shown in figure 7. It will be noted that there is a corresponding minimum of the total lift as shown in figure 8, and that this maximum reduction in lift due to the afterbody is a sizable fraction of the total lift.

Figure 6 indicates that the lift per unit wing incidence carried on the afterbody is positive for small $\delta_W \frac{d}{s_o}$ and negative for large $\delta_W \frac{d}{s_o}$. Also, an increase of the afterbody length apparently always results in a reduction of lift for short afterbodies. However, the actual values must be viewed with caution near $\delta_W \frac{d}{s_o} = 0$ since figure 8 shows an inconsistency there. That is, the total lift per unit wing incidence for no afterbody $\left(\delta_W \frac{d}{s_o} = 0\right)$, according to the present theory, does not agree

with $\frac{L_{WB}}{\delta_W}$ as given by equation (43). The reason for this discrepancy is the assumption here that the vortex sheet is fully rolled up at $x = l$. That is, the present analysis is applicable only to combinations having an afterbody length at least as great as the distance required for the vortex sheet to become fully rolled up.

An estimate of the distance e for rolling up of the vortex sheet can be obtained directly from the formula given in reference 11

$$\frac{e}{2s} = k_1 \frac{A}{C_L} = \frac{k_1}{C_L}\left(\frac{4s^2}{S_W}\right) \tag{44}$$

provided that we replace s by $(s_o - a)$. In this manner, using equations (15) and (16) and replacing C_L by $\frac{L_W}{\frac{1}{2}\rho U_o^2 S_W}$, we find

$$\delta_W \frac{e}{s_o} = \frac{\pi k_1 \left(1 - \frac{a}{s_o}\right)^2}{\left(\frac{y_{1_{TE}}}{s_o} - \frac{a}{s_o}\right)\left(1 + \frac{a}{s_o}\right)\left[\frac{\pi}{2} + \cos^{-1}\left(\frac{2\frac{a}{s_o}}{1 + \frac{a^2}{s_o^2}}\right)\right]} \tag{45}$$

Now Kaden (ref. 14) has given a value for k_1 of 0.28 for wings with elliptic circulation distribution, but in reference 15 it has been pointed out that this value is much too low to agree with numerical calculations. For our purpose here, namely to obtain an estimated lower limit for $\delta_W \frac{d}{s_o}$ of the present calculations, it will be sufficient to take twice Kaden's value; that is, $k_1 = 0.56$. That this is a reasonable choice can be verified by comparing with the numerical results of reference 16 for a plane wing.

The values of $\delta_W \frac{d}{s_o}$ for rolling up of the vortex sheet, as given by equation (45) using $k_1 = 0.56$, have been calculated and the curves of figure 8 have been modified by the dashed lines to agree with L_{WB} at $\delta_W \frac{d}{s_o} = 0$. It can be seen that a short afterbody is still expected to give positive lift, as indicated by figure 6. However, the curves of figure 6 should actually pass through the origin in agreement with the dashed curves of figure 8. It then becomes clear that the afterbody lift has a positive maximum at some small $\delta_W \frac{d}{s_o}$ as well as a negative maximum at a rather large $\delta_W \frac{d}{s_o}$.

Another indication of the error at small values of $\delta_W \frac{d}{s_o}$ is given by the curve for $\delta_W \frac{d}{s_o}$ of zero in figure 7. Since this curve should actually coincide with the axis (i.e., it should indicate no lift on an afterbody of zero length), the values shown are a direct measure of the error involved. This error is of course a maximum at $\delta_W \frac{d}{s_o} = 0$ and diminishes to zero at $\delta_W \frac{e}{s_o}$ as shown in figure 8.

It might be of interest to consider for a moment the physical significance of the discrepancy discussed above between the present theory and ordinary slender-body theory for small values of $\delta_W \frac{d}{s_o}$ (i.e., for short afterbodies). Ordinarily, in discussions of the rolling up of the vortex sheet behind a wing, we make frequent use of the fact that the lift impulse is unchanged during the rolling-up process. The reason for this invariance, of course, is the absence of a body capable of sustaining a force in the wake. For the problem treated here, however, such a body is present in the wake, the lift impulse varies with distance downstream, and there is a force carried on the body just due to the rolling up of the vortex sheet. It is in fact just this lift which is the value indicated in figures 6 and 7 at $\delta_W \frac{d}{s_o} = 0$, and it is seen that this lift is positive in all cases.

In figure 9, the calculated curves of total lift as a function of wing incidence are presented for a number of wing-body-afterbody combinations. The lift curves are, as expected, increasingly nonlinear as the body-diameter to wing-span ratio is increased and as the afterbody length is increased.

Now since equation (12) was actually developed for wing-body-tail combinations, assuming that the tail has no influence on the vortex positions, we can calculate the total lift for such combinations directly from that equation. The strengths and positions of the rolled-up vortices are again given by equations (16) and (39) and the length d now becomes the tail length, that is, the distance between the trailing edges of wing and tail. The calculated lift curves are presented in figures 10 and 11 for two ratios of tail span to wing span, one less than 1 and one greater than 1. In both cases, the tail is at zero incidence so that $L_{BT} = 0$. For other tail incidences, L_{BT} is given in reference 10.

In figure 10 the tail span is half the wing span and the lift curves for the smallest body radius shown ($a/s_o = 0.2$) are almost linear for all the tail lengths calculated. The curves evidently become increasingly nonlinear as the body radius is increased and as the tail length is increased. For the largest body radius ($a/s_o = 0.8$) and the longest tail length ($d/s_o = 24$), the lift curve slope changes sign at a fairly small angle of incidence ($\delta_W \approx 8.5^\circ$). If the tail span is somewhat greater than

the wing span (e.g., $s_1/s_o = 1.5$, fig. 11), the lift curves are more nonlinear and the effect of increasing the tail length is more pronounced.

CONCLUDING REMARKS

A theoretical analysis has been made of the lift produced on the afterbody and tail of a slender plane wing-body-tail combination at zero angle of attack due to incidence of the wing. It was assumed throughout the analysis that the vortex sheets leaving the wing panels become fully rolled up ahead of the trailing edge of the tail or the base of the afterbody.

The lift produced on the afterbody with no tail was found to have a positive maximum at a certain short afterbody length and a negative maximum at a certain very large afterbody length. The rolling up of the vortex sheet was found to produce a positive lift on the afterbody.

The total lifts of some plane wing-body-tail combinations having tail spans less than and greater than the wing span were calculated, and the lift curves were found to become increasingly nonlinear as the ratio of body diameter to wing span was increased.

The lift due to wing incidence as calculated in the present report cannot be added directly to the lift of the body at angle of attack since inclining the body would alter the paths of the rolled-up vortices. As a matter of fact, if the angle of attack of the body is not zero, the path of the integration required to relate the vortex positions to the distance behind the wing becomes transcendental rather than algebraic as in the present case. Therefore, application of the methods employed here does not seem feasible for problems in which the body is not aligned with the flight direction.

Ames Aeronautical Laboratory
National Advisory Committee for Aeronautics
Moffett Field, Calif., Aug. 14, 1956

REFERENCES

1. Graham, Martha E.: Some Linearized Computations of Supersonic Wing-Tail Interference. Rep. SM-13430, Douglas Aircraft Co., Inc., Santa Monica, Dec. 23, 1948.

2. Morikawa, George: Supersonic Wing-Body-Tail Interference. Jour. Aero. Sci., vol. 19, no. 5, May 1952, pp. 333-340.

3. Sacks, Alvin H.: Aerodynamic Interference of Slender Wing-Tail Combinations. NACA TN 3725, 1956.

4. Lagerstrom, Paco A., and Graham, Martha E.: Aerodynamic Interference in Supersonic Missiles. Rep. SM-13743, Douglas Aircraft Co., Inc., Santa Monica, July 1950.

5. Rogers, Arthur W.: Application of Two-Dimensional Vortex Theory to the Prediction of Flow Fields Behind Wings of Wing-Body Combinations at Subsonic and Supersonic Speeds. NACA TN 3227, 1954.

6. Milne-Thomson, L. M.: Theoretical Hydrodynamics. Second ed., MacMillan Co., N. Y., 1950.

7. Villat, H.: Lecons sur la Theorie des Tourbillons Gauthier-Villars, Paris, 1930.

8. Sacks, Alvin H.: Vortex Interference on Slender Airplanes. NACA TN 3525, 1955.

9. Ward, G. N.: Linearized Theory of Steady High-Speed Flow. Cambridge Univ. Press, 1955.

10. Dugan, Duane W., and Hikido, Katsumi: Theoretical Investigation of the Effects Upon Lift of a Gap Between Wing and Body of a Slender Wing-Body Combination. NACA TN 3224, 1954.

11. Spreiter, John R., and Sacks, Alvin H.: The Rolling Up of the Trailing Vortex Sheet and Its Effect on the Downwash Behind Wings. Jour. Aero. Sci., vol. 18, no. 1, Jan. 1951, pp. 21-32, 72.

12. Byrd, Paul F., and Friedman, Morris D.: Handbook of Elliptic Integrals for Engineers and Physicists. Die Grundlehren der Mathematischen Wissenschaften, Band LXVII, Springer-Verlag, Berlin, 1954.

13. Adams, Edwin P.: Smithsonian Mathematical Formulae and Tables of Elliptic Functions. Smithsonian Miscellaneous Collections, vol. 74, no. 1, 1947.

14. Kaden, H.: Aufwicklung einer unstabilen Unstetigkeitsflache. Ing.-Archiv, Bd. II, 1931, pp. 140-168.

15. Spreiter, John R., and Sacks, Alvin H.: A Theoretical Study of the Aerodynamics of Slender Cruciform-Wing Arrangements and their Wakes. NACA TN 3528, 1956.

16. Westwater, F. L.: Rolling Up of the Surface of Discontinuity Behind an Aerofoil of Finite Span. R. and M. No. 1692, British A.R.C., August 1955.

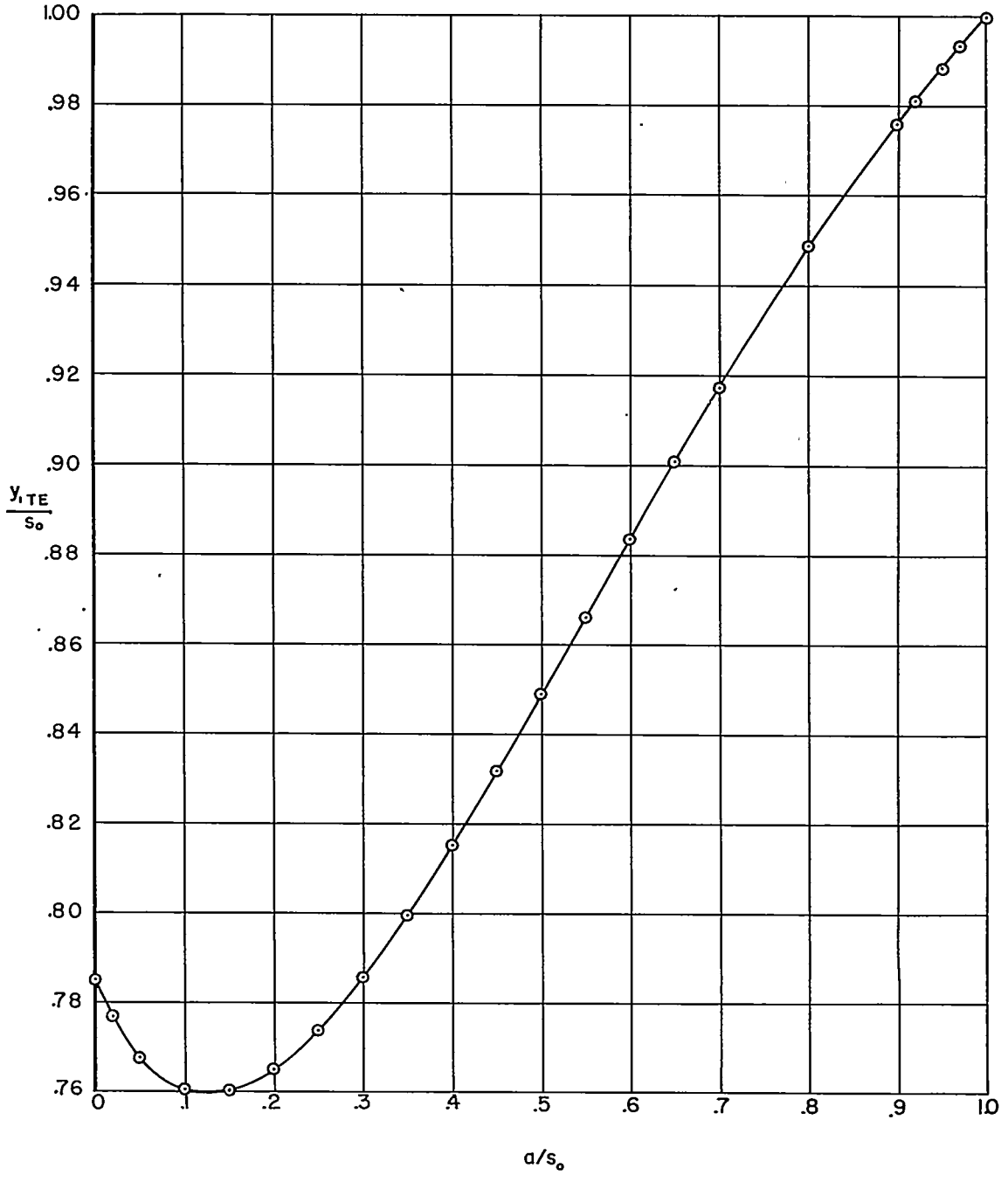

Figure 1.- Lateral position of starboard vortex at wing trailing edge; plane wing-body-tail combination, $\alpha = 0$, $\delta_w \neq 0$, (eq. (18)).

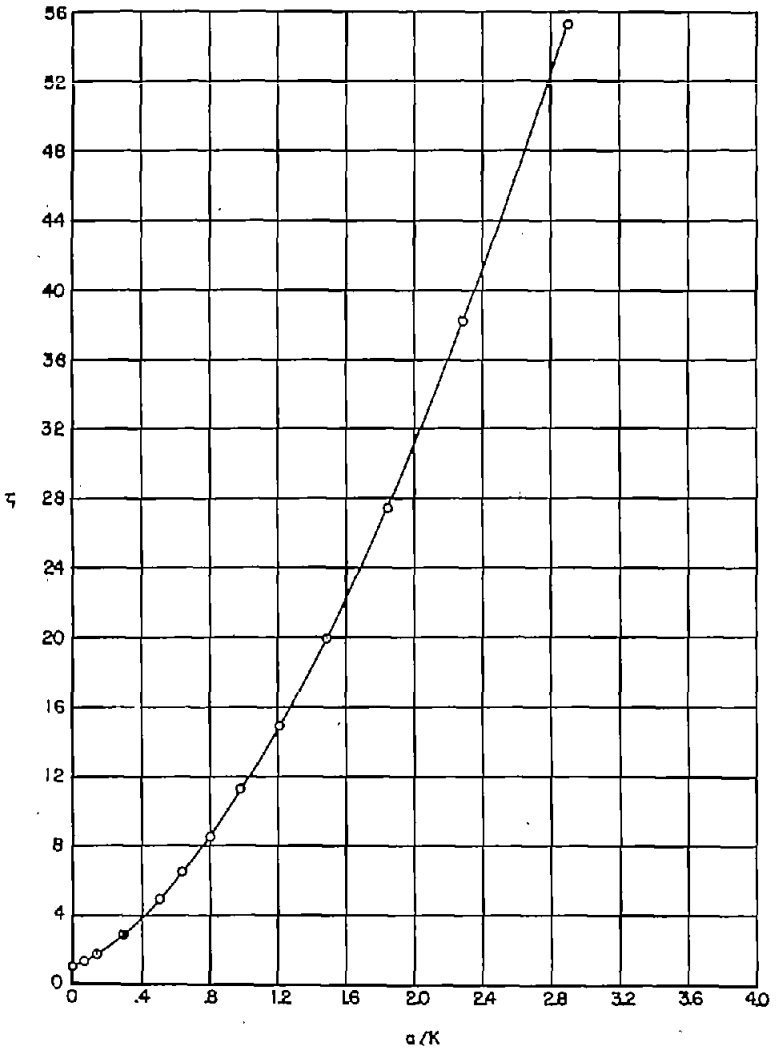

(a) τ_1

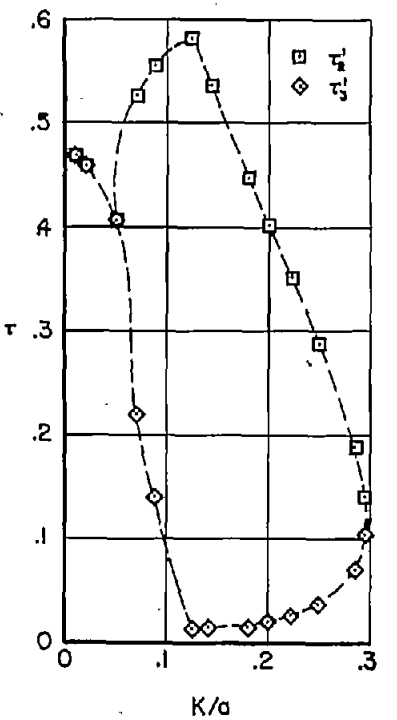

(b) τ_2' and τ_3'

Figure 2.- Roots of polynomial $P(\tau)$ according to equations (32) and (33).

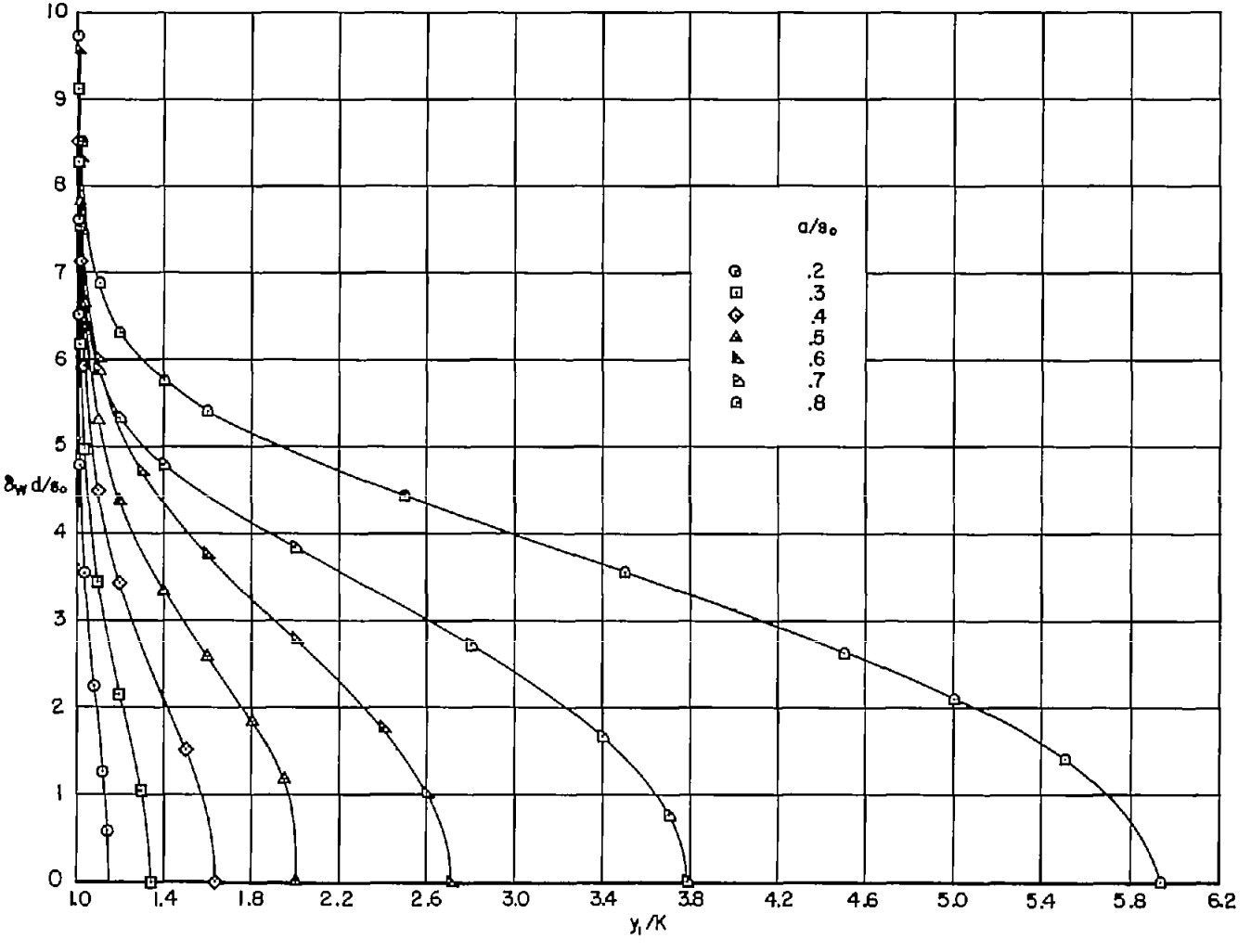

Figure 3.- Effect of body-radius to wing-semispan ratio and afterbody length on lateral position of starboard vortex at $x = l$; $\alpha = 0$, $\delta_w \neq 0$, (eq. (39)).

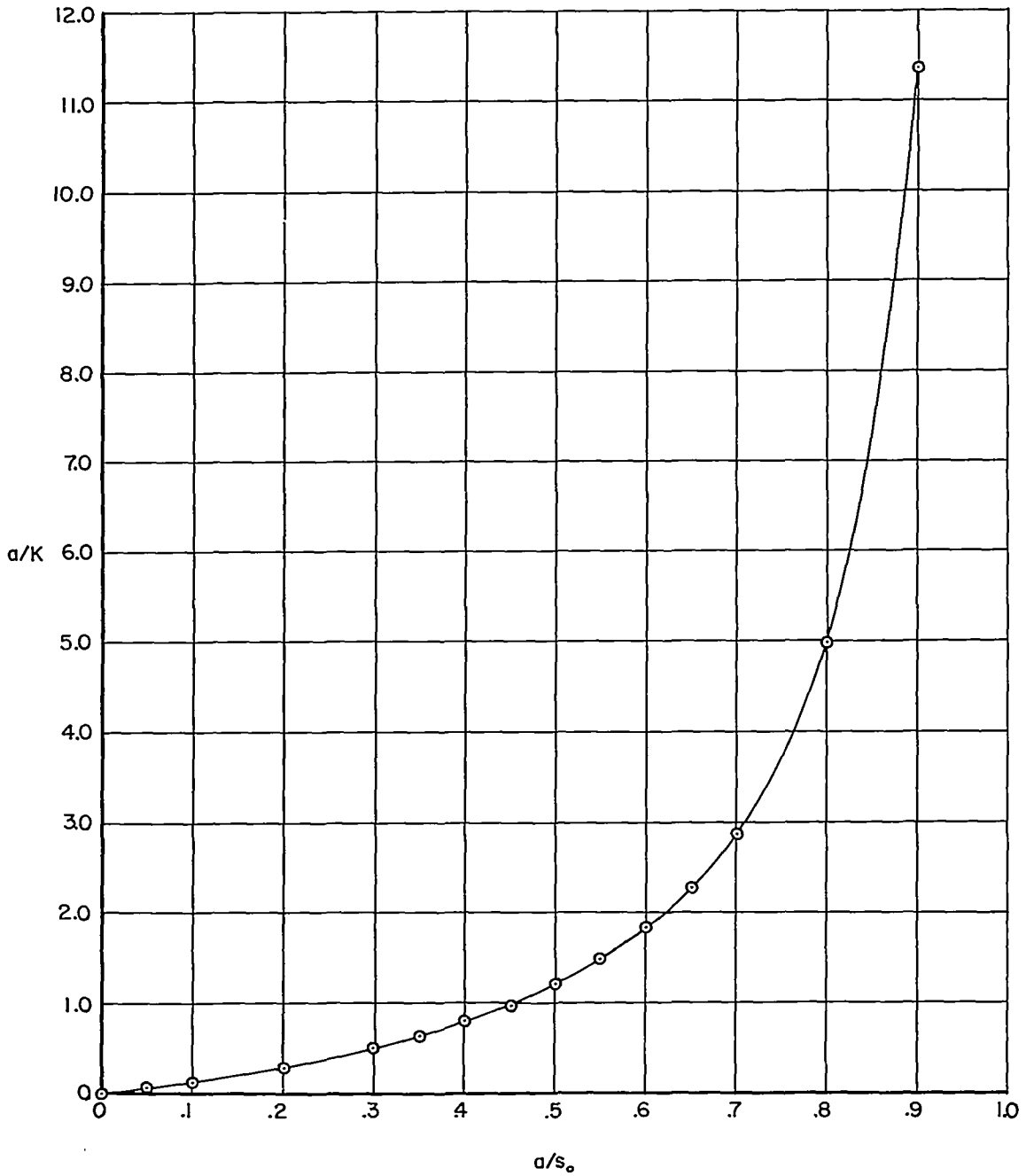

Figure 4.- Equations (35) and (18).

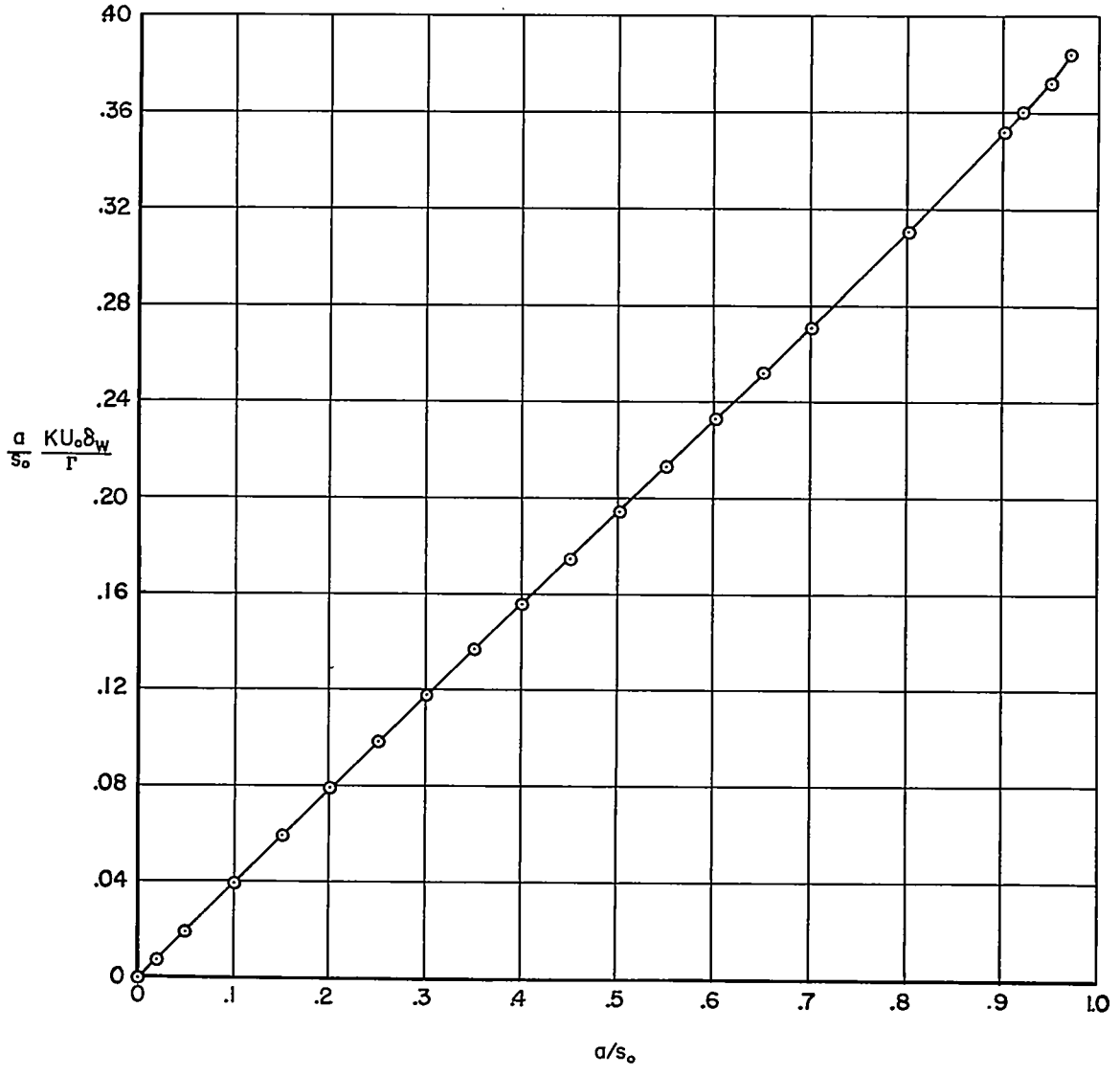

Figure 5.- Equations (35) and (16).

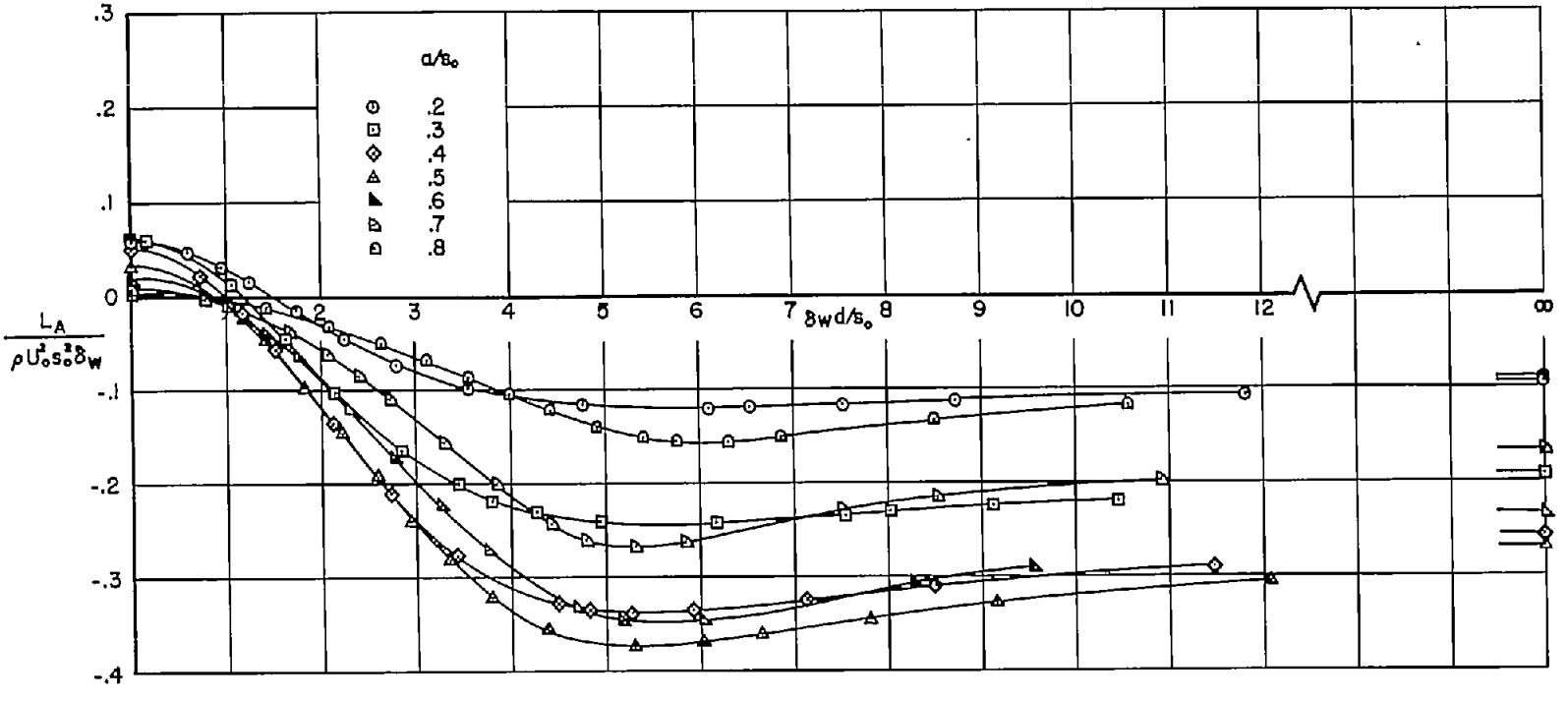

Figure 6.- Effect of body-radius to wing-semispan ratio on the variation of afterbody lift with afterbody length and wing incidence; $\alpha = 0$, $\delta_w \neq 0$.

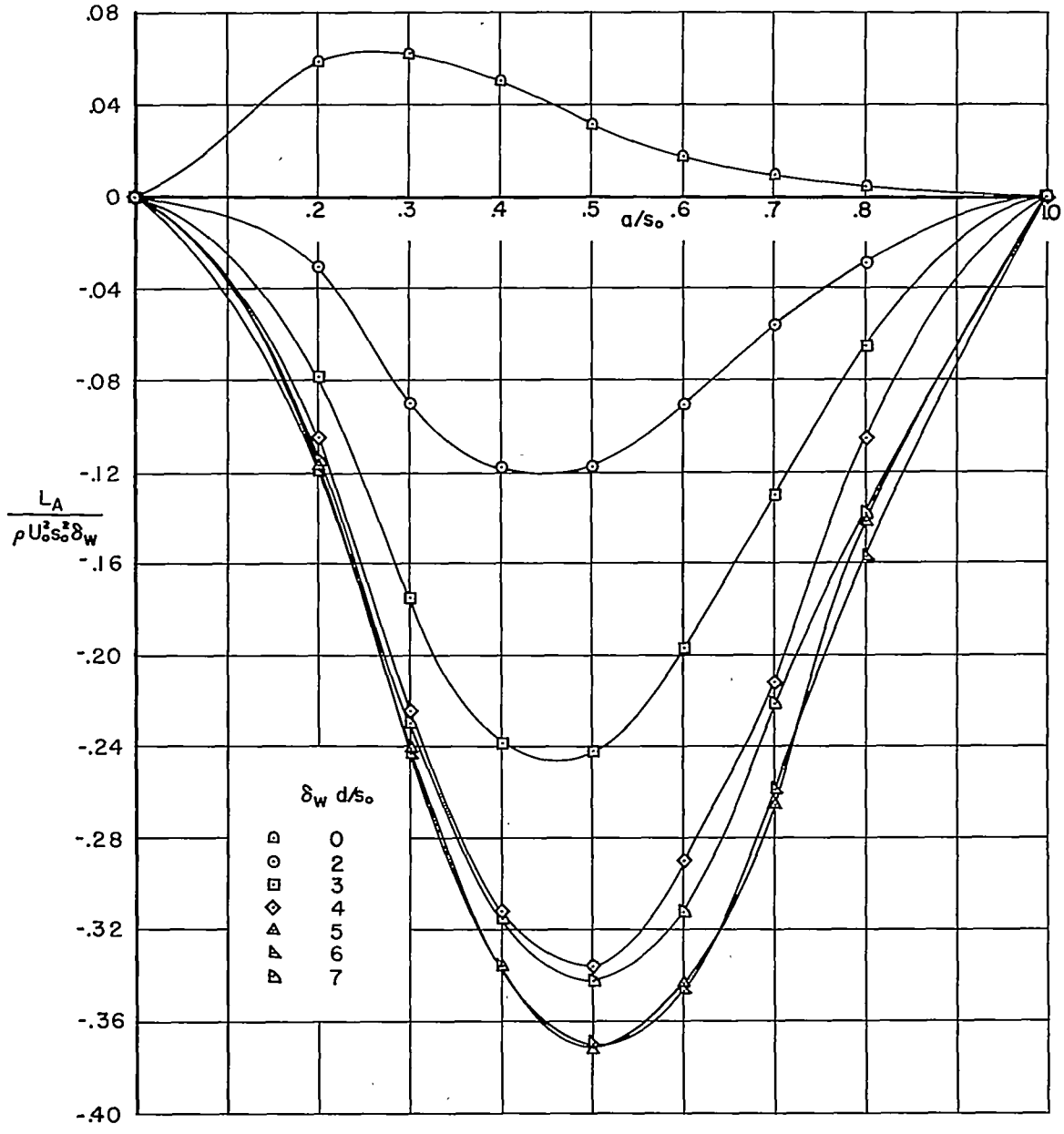

Figure 7.- Effect of afterbody length and wing incidence on the variation of afterbody lift with ratio of body radius to wing semispan; $\alpha = 0$, $\delta_w \neq 0$.

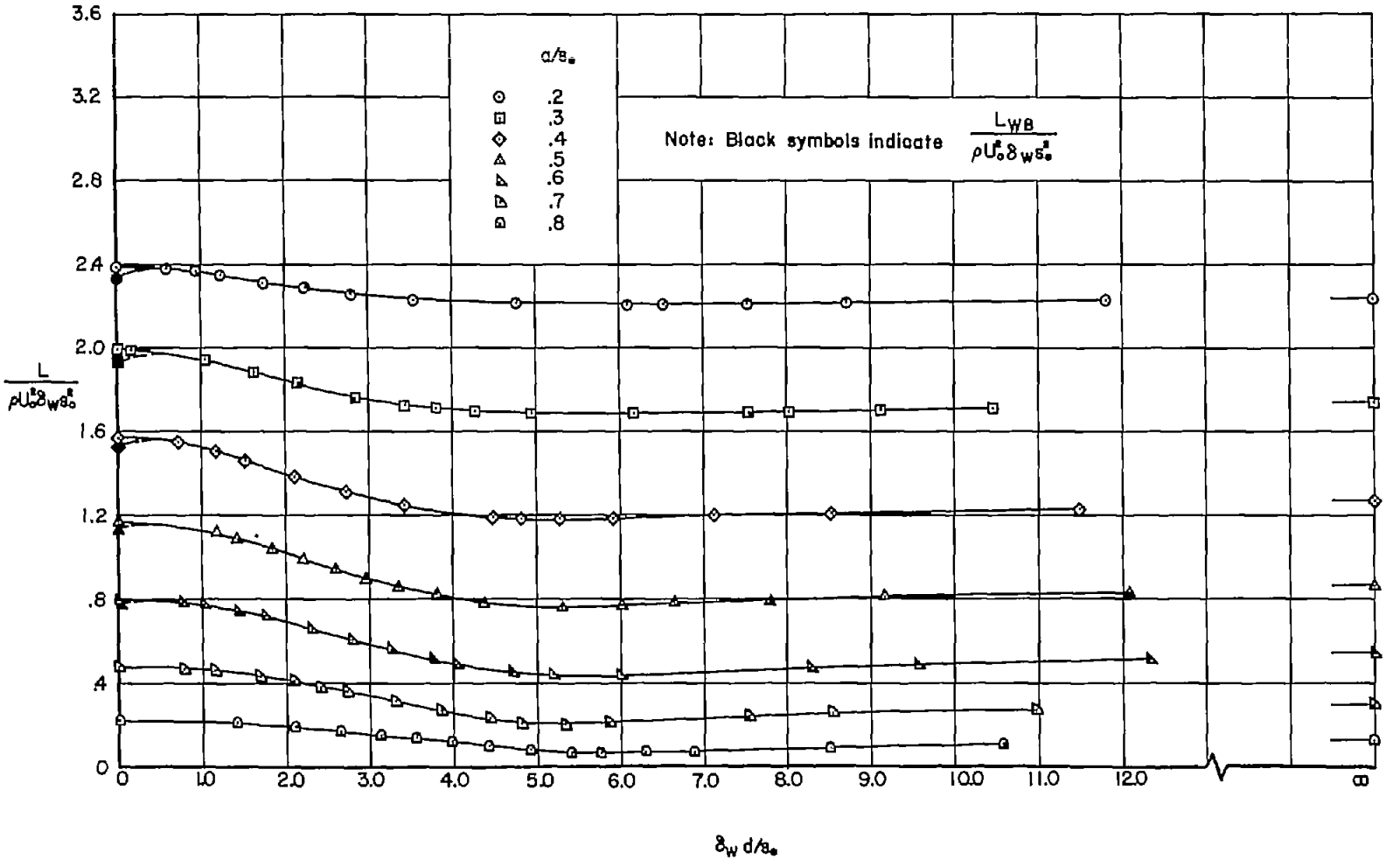

Figure 8.- Effect of body-radius to wing-semispan ratio on the variation of total lift with afterbody length and wing incidence; plane wing-body-afterbody combination, $\alpha = 0$, $\delta_w \neq 0$.

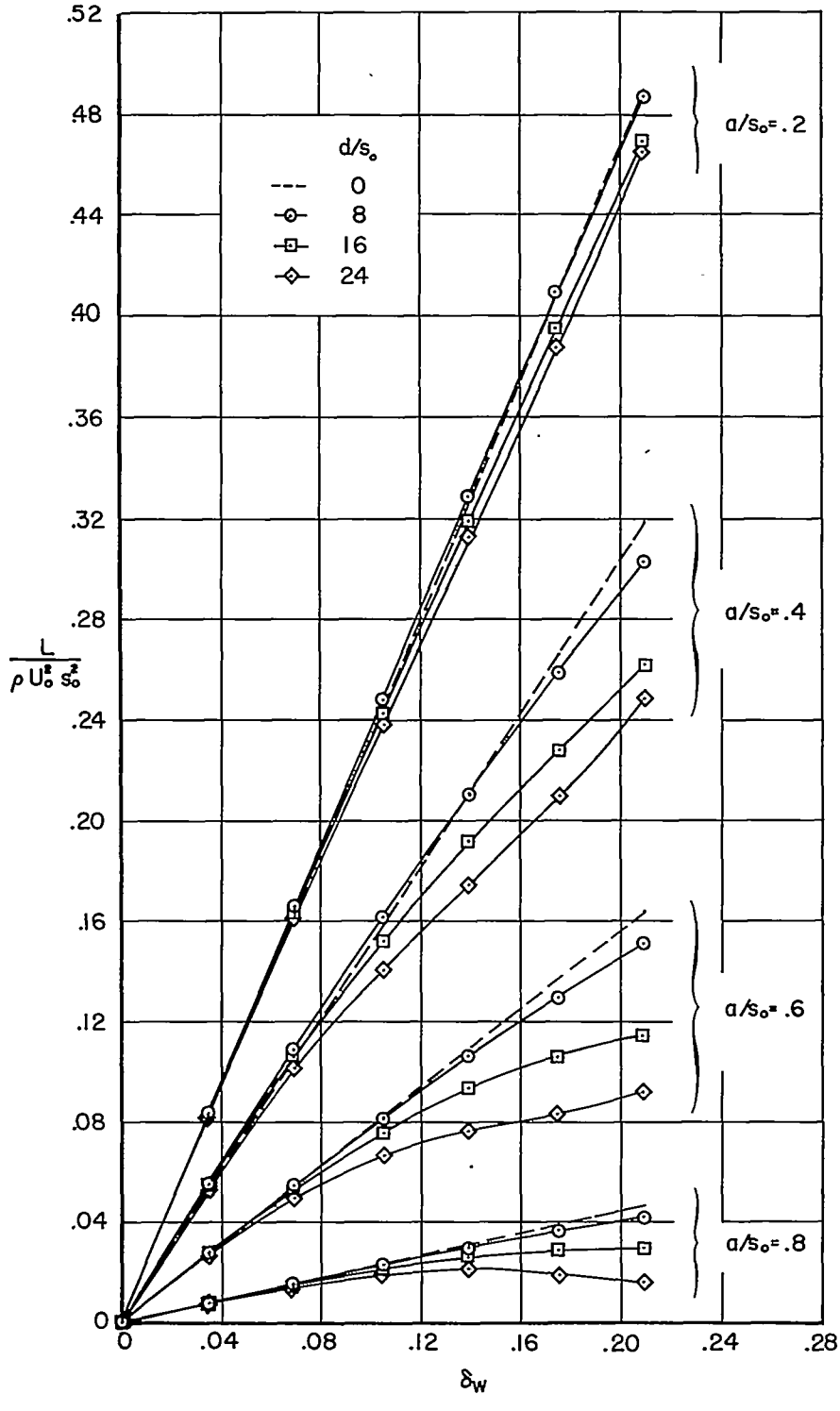

Figure 9.- Effect of body-radius to wing-semispan ratio and afterbody length on the variation of total lift with wing incidence; plane wing-body-afterbody combination, $\alpha = 0$, $\delta_w \neq 0$.

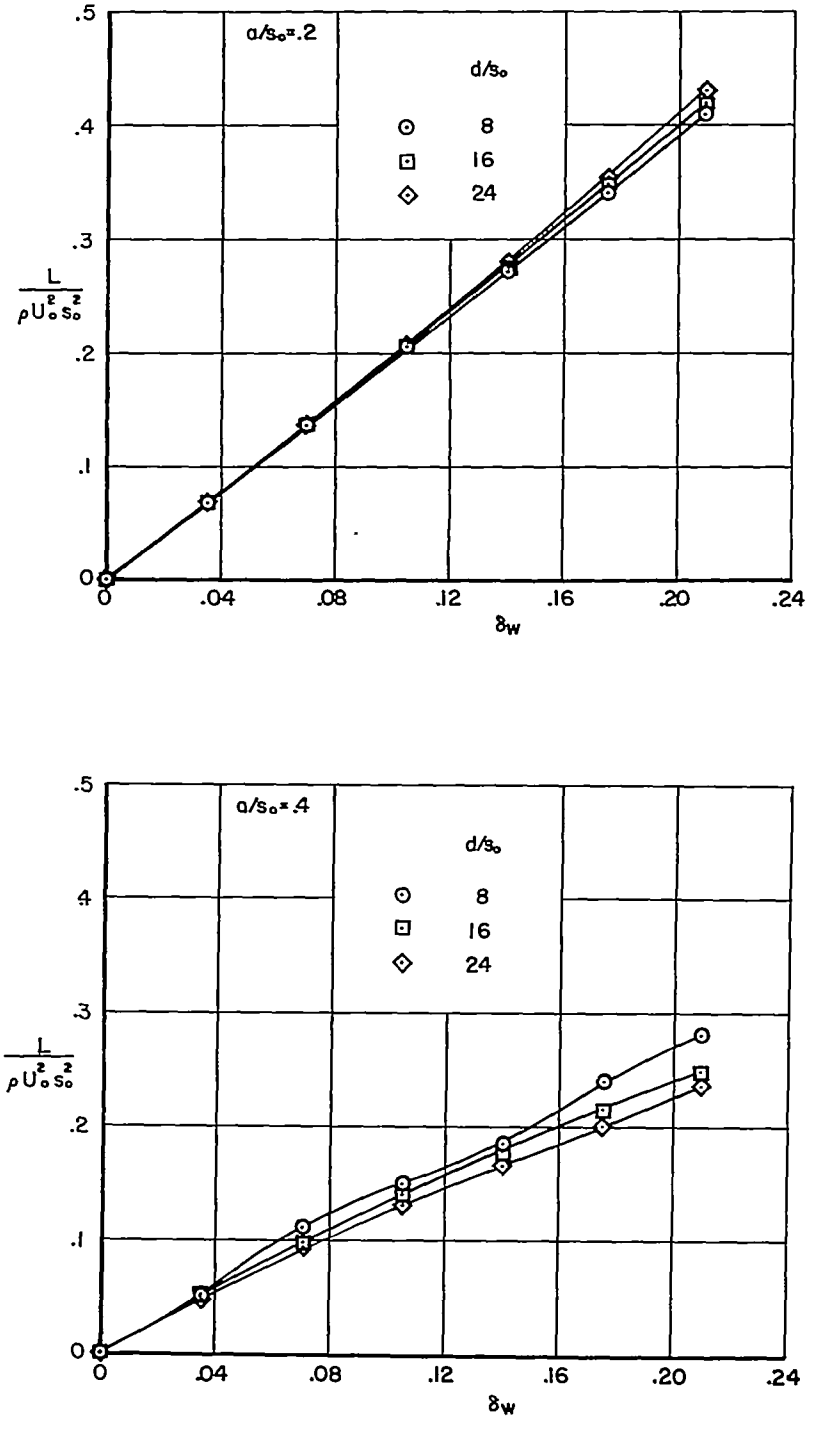

(a) a/s = 0.2, 0.4

Figure 10.- Effect of body-radius to wing-semispan ratio and tail length on the variation of total lift with wing incidence; plane wing-body-tail combination, $\alpha = 0$, $\delta_T = 0$, $\delta_W \neq 0$, $s_1/s_0 = 0.5$.

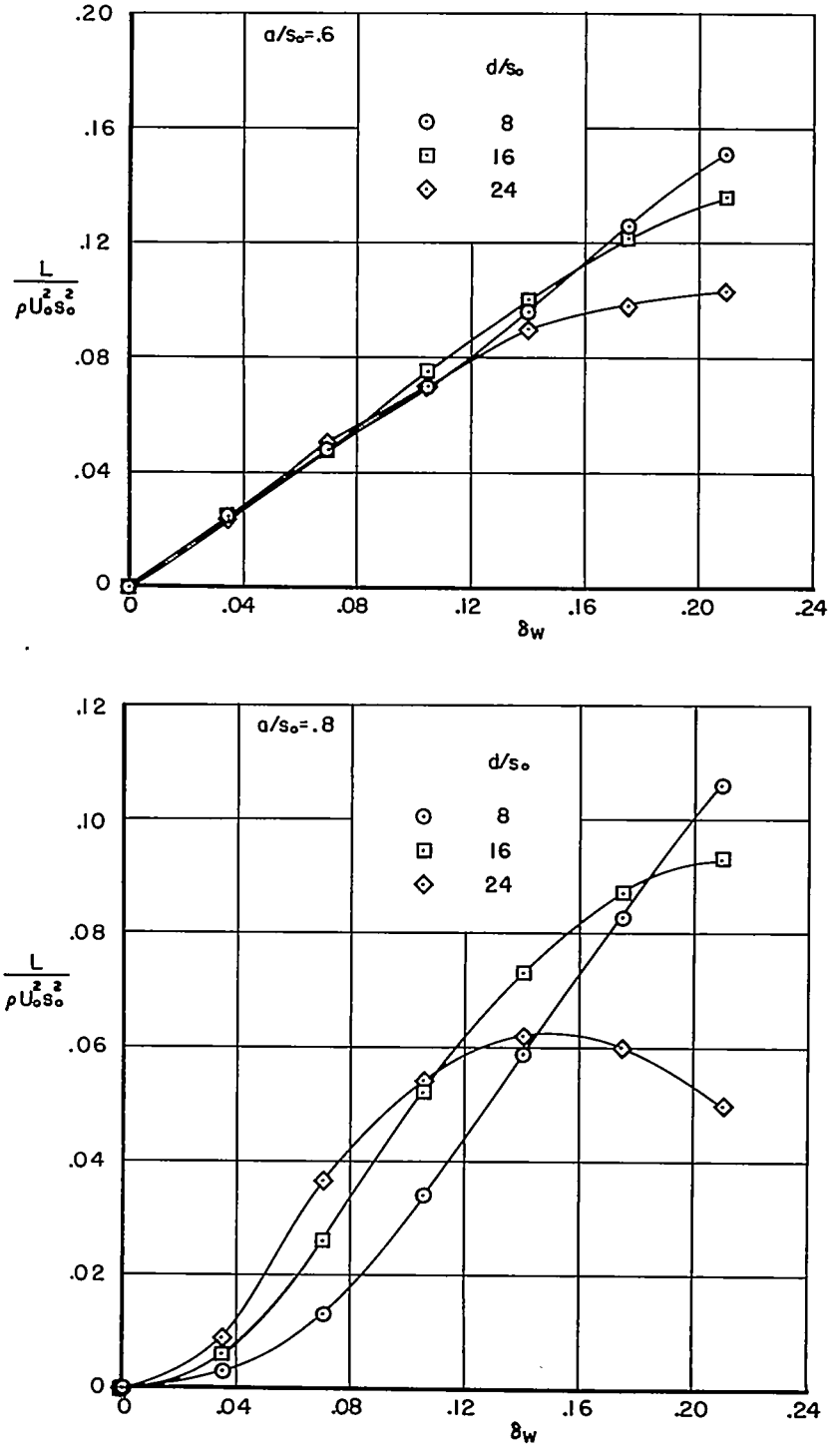

(b) a/s = 0.6, 0.8

Figure 10.- Concluded.

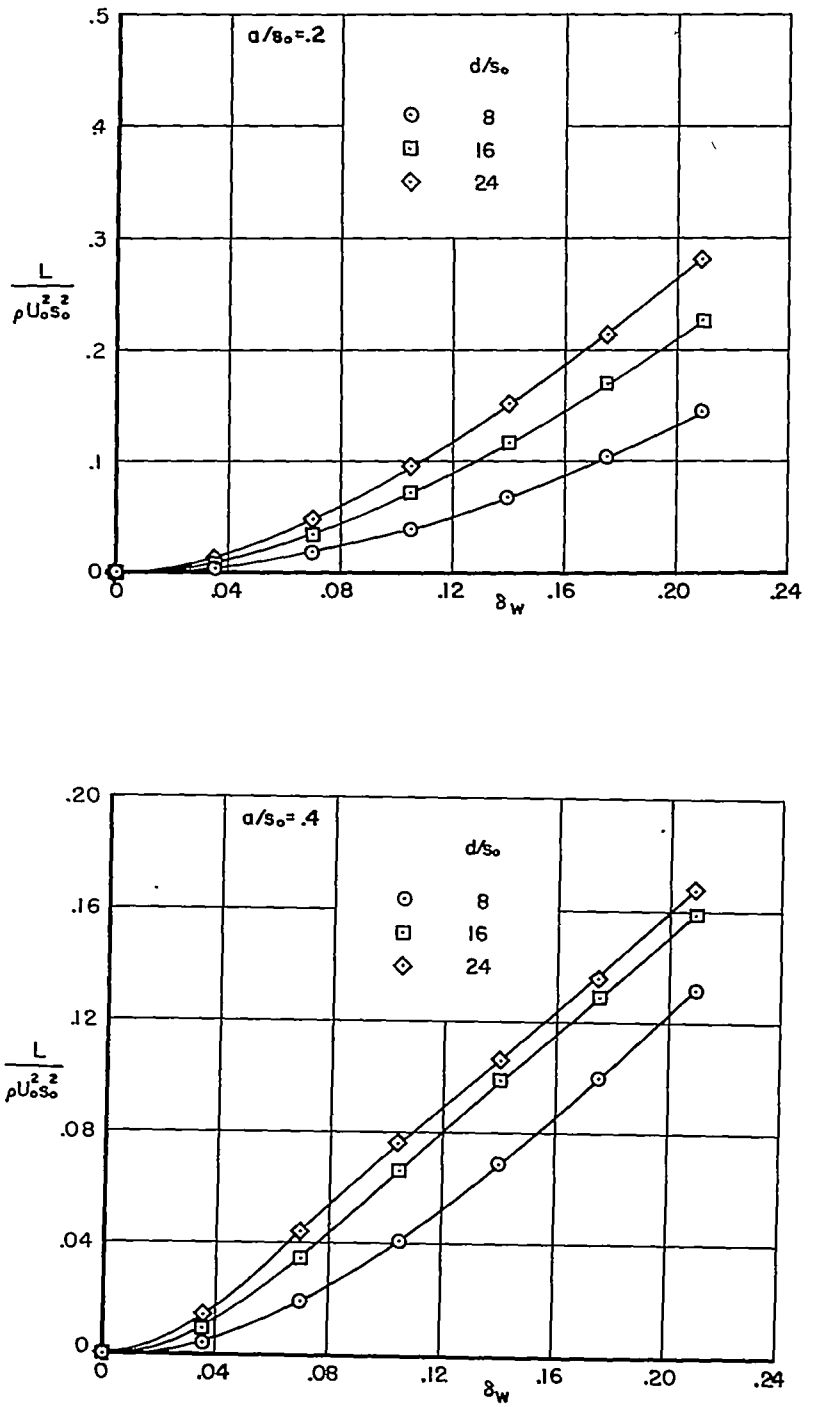

(a) a/s = 0.2, 0.4

Figure 11.- Effect of body-radius to wing-semispan ratio and tail length on the variation of total lift with wing incidence; plane wing-body-tail combination, $\alpha = 0$, $\delta_T = 0$, $\delta_W \neq 0$, $s_1/s_0 = 1.5$.

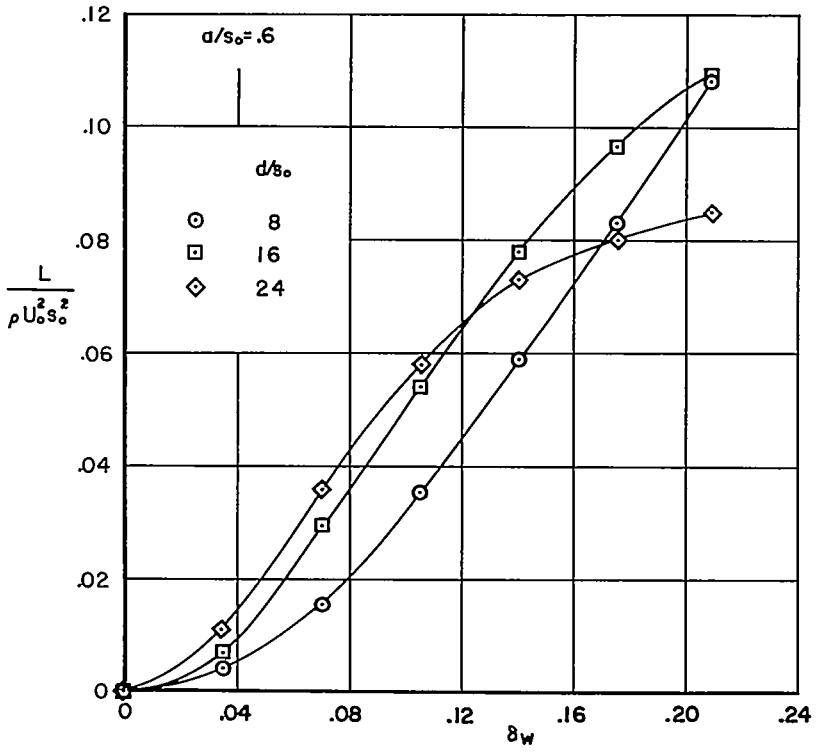

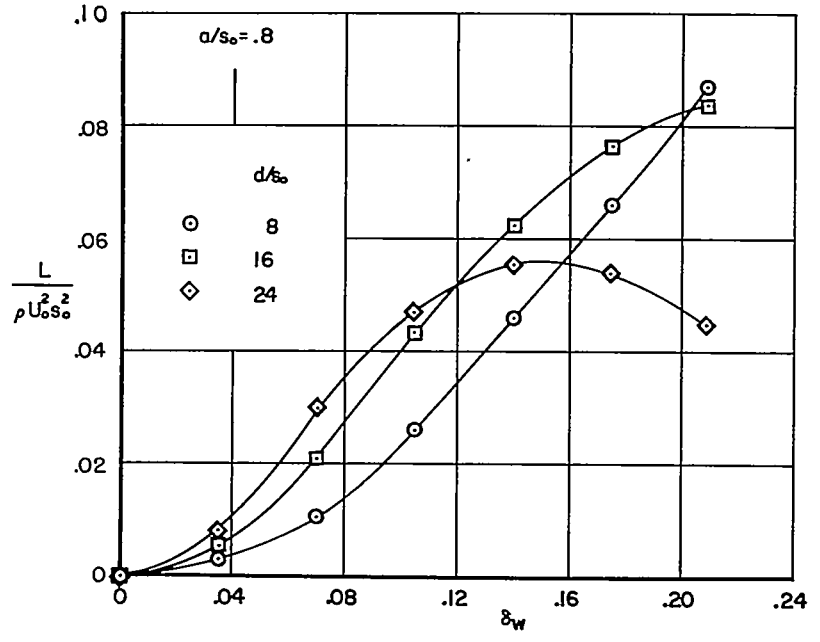

(b) a/s = 0.6, 0.8

Figure 11.- Concluded.